doi:10.1093/jmcb/mju049
Published online December 29, 2014

Article

Cigarette smoke-induced cell cycle arrest in spermatocytes [GC-2spd(ts)] is mediated through crosstalk between *Ahr–Nrf2* pathway and MAPK signaling

Prabagaran Esakky[1,2], Deborah A. Hansen[1], Andrea M. Drury[1,2], and Kelle H. Moley[2,*]

[1] Research, Department of Veterans Affairs Medical Center, St. Louis, MO 63106, USA
[2] Department of Obstetrics and Gynecology, Washington University School of Medicine, St. Louis, MO 63110, USA
* Correspondence to: Kelle H. Moley; E-mail: moleyk@wustl.edu

Our earlier studies have demonstrated that the cigarette smoke in the form of cigarette smoke condensate (CSC) causes growth arrest of a mouse spermatocyte cell line [GC-2spd(ts)] through activation of the AHR–NRF2 pathway. The present study demonstrates the CSC-activated p38 and ERK MAPK signaling in GC-2spd(ts) via arylhydrocarbon receptor (AHR). Pharmacological inhibition by using AHR-antagonist, or p38 MAPK and ERK (MEK1) inhibitors significantly abrogates CSC-induced growth arrest by AHR and MAPK inactivation. QRT-PCR, western blot, and immunofluorescence of *Ahr*-target of *Nrf2*, and stress-inducible growth suppressive *Atf3* and *E2f4* following treatments indicate a crosstalk among these pathways. Regulation of *Atf3* by *Nrf2* and *Ahr* through RNA interference suggests the existence of a cross-regulatory loop between the targets. CSC induction of *E2f4* via *Atf3* and its regulation by pharmacological inhibitors reveal a possible regulatory mechanism of growth inhibitory CSC. SiRNA silencing of *Ahr*, *Nrf2*, *Atf3*, and *E2f4* genes and downregulation of cyclins by CSC corroborate the growth inhibitory effect of cigarette smoke. Thus, the data obtained suggest that the CSC-mediated MAPKs and AHR–NRF2 crosstalks lay the molecular basis for the growth arrest and cell death of spermatocytes.

Keywords: spermatocytes, *Ahr*, *Nrf2*, CSC, ATF3, E2F4, p38 MAPK, and ERK

Introduction

Cigarette smoke contains >4000 chemicals including 60 proven carcinogens (Smith et al., 2003). Toxic constituents of cigarette smoke accumulating in the systemic circulation and seminal plasma deleteriously affect sperm viability and fertility (Ramlau-Hansen et al., 2007). Chronic exposures to cigarette smoke cause testicular toxicity (Georgellis et al., 1987) and male infertility (Aitken and Baker, 2004). However, the molecular basis that governs the generation of dysfunctional germ cells by male smokers remains unclear.

Dioxins and polycyclic aromatic hydrocarbons (PAHs) including benzo(a)pyrene (B[a]P) and semiquinones (Smith and Hansch, 2000) majorly constitute the cigarette smoke condensate (CSC), or tar. Oxidative stress generated by CSC perniciously alters *p21, Gadd45a, Sod2*, *IL-1β, Cyp1a1, Hsp90aa1* genes, etc. in various cell and tissue types including spermatocytes (Fields et al., 2005; Esakky et al., 2012, 2014). CSC exposure in oral cancer cells stimulates genes involved in the metabolism of PAHs (Nagaraj et al., 2006). TCDD (2,3,7,8-Tetrachlorodibenzo-*p*-dioxin) and the PAHs exert growth modulation by binding to the ligand-dependent AHR (Hoffman et al., 1991). These AHR agonists and its metabolites in CSC transactivate AHR, which in turn regulates target genes through dioxin response elements (Kumar et al., 1999). Similarly, reactive oxygen species (ROS) activate nuclear factor-erythroid 2-related factor 2 (*Nrf2*), which regulates target genes via antioxidant response elements (Venugopal and Jaiswal, 1996). Dioxins and B[a]P also activate multiple cellular signaling, although their mechanistic influence on a particular pathway has not been well established. Several signaling pathways target AHR including proteasomal degradation (Pollenz and Buggy, 2006), redox-sensitive transcription factors (Zordoky and El-Kadi, 2009), and the mitogen-activated protein kinases (MAPKs) (Henklová et al., 2008). Among multiple groups of MAPKs, the best studied are the extracellular signal-regulated kinases (ERKs), p38, and Jun-NH2-terminal kinase (JNK) MAPK pathways. These MAPKs elicit cell-specific gene expressions through downstream transactivators by phosphorylation (Davis, 2000).

AHR activators such as TCDD and B[a]P act as inducers of MAPKs (Henklová et al., 2008), suggesting MAPKs as connecting link

Received June 15, 2014. Revised October 7, 2014. Accepted October 20, 2014.

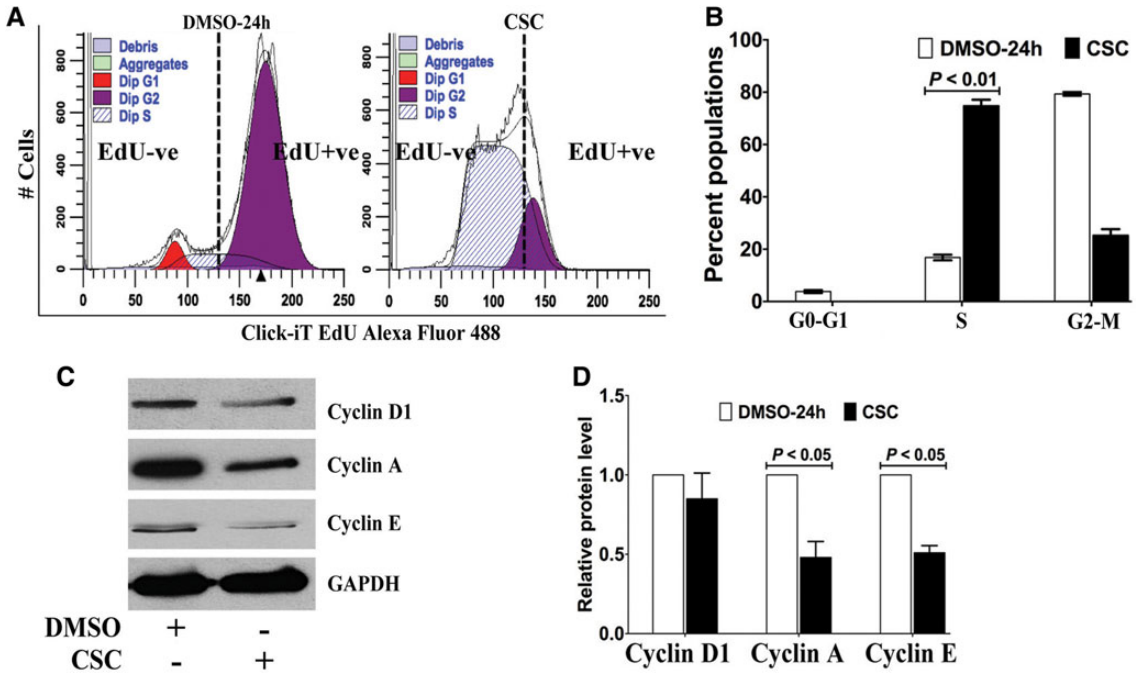

Figure 1 CSC inhibits DNA synthesis and cell proliferation. (**A**) Spermatocytes exposed to DMSO (0.1%) or CSC (100 μg/ml) for 24 h were assessed for DNA synthesis by EdU Click-iT Assay. EdU incorporation into DNA was evaluated by using a FACScalibur flow cytometer (Becton-Dickinson) and the data were analyzed using the BD Modfit LT (V4.0.5) software. Broken lines separate the EdU^{+ve} (EdU-positive) from EdU^{-ve} (EdU-negative) populations. (**B**) The histogram represents the mean ± SEM of flow cytometric data of treated samples at G0/G1, S, and G2/M phases of three independent experiments assayed in triplicates. (**C**) Western blot analysis of GC-2spd(ts) cells treated with DMSO (0.1%) or CSC (100 μg/ml) for 24 h. The protein extracted was probed with anti-cyclin D1, anti-cyclin A, and anti-cyclin E antibodies and the blots were reprobed with anti-glyceraldehyde-3-phosphate dehydrogenase (GAPDH) for uniform loading. (**D**) The histogram represents cyclin D1, cyclin A, and cyclin E levels in relative densitometric units normalized to GAPDH ($n = 3$).

between AHR and various physiological processes. For example, TCDD-stimulated MAPKs appear critical for induction of AHR-dependent *Cyp1a1* expression (Tan et al., 2002). It also appears that AHR ligands activate the MAPKs in a cell- or tissue-specific manner, and that the kinase in turn regulates AHR, facilitating the transactivation of target genes. The increase in the transcriptional activity of ELK and JUN respectively, by TCDD-activated ERK, p38, and JNK MAPKs established a novel mode of AHR action and its 'crosstalking' with these MAPKs (Tan et al., 2002; Weiss et al., 2005). This indicates a two-way crosstalk between MAPK pathways and AHR signaling.

The present study tested the hypothesis that AHR ligands of CSC cause immediate activation of ERK and p38 MAPKs, which plays a crucial role in AHR function. The findings of the current study clearly show that CSC activates p38 and ERK MAPKs with the help of AHR, and that the activated MAPK is essential for AHR-dependent gene regulation. Application of specific pharmacological inhibitors reveals how inactivation of AHR and MAPK pathways enables cell cycle progression of spermatocytes arrested by CSC. Following activation, the potential downstream target of AHR, *Nrf2* regulates *Atf3* expression. We noticed here that both the CSC-induced *Atf3* and its downstream E2F4 undergo multiple regulations and the changes to *E2f4* might be responsible for the growth inhibition of spermatocytes. In addition, the suppression of candidate genes by RNA interference alludes to the fact that the AHR–NRF2–ATF3–E2F4 pathway is playing a vital role in accurate growth transition of spermatocytes besides cyclins. Thus, the data presented in the manuscript suggest that the activation of MAPKs could be one of the essential regulatory features of AHR ability to function as a CSC-responsive transcription factor.

Results

CSC blocks DNA synthesis at S-phase

Our previous study showed the CSC-mediated accumulation of GC-2spd(ts) spermatocytes in the S-phase (Esakky et al., 2014). To confirm whether the cells accumulate due to blockade in DNA synthesis, we performed EdU incorporation assay followed by flow cytometry, which showed that the number of EdU^{-ve} (EdU-negative, nonproliferative) spermatocyte populations increased significantly (~75%; $P < 0.01$) at S-phase following CSC treatment (Figure 1A and B). Western blot demonstrated that CSC has also significantly downregulated ($P < 0.05$) cyclins A and E in spermatocytes (Figure 1C and D). These results clearly reiterate our notion that CSC induces S-phase arrest by inhibiting DNA replication and downregulating G1-S phase cyclins.

CSC induces crosstalk between AHR and MAPKs

As the constituents of CSC can modulate AHR and other signaling, we evaluated the activation of p38 and ERK MAPKs by western blot in GC-2spd(ts). As seen in Figure 2A, CSC significantly

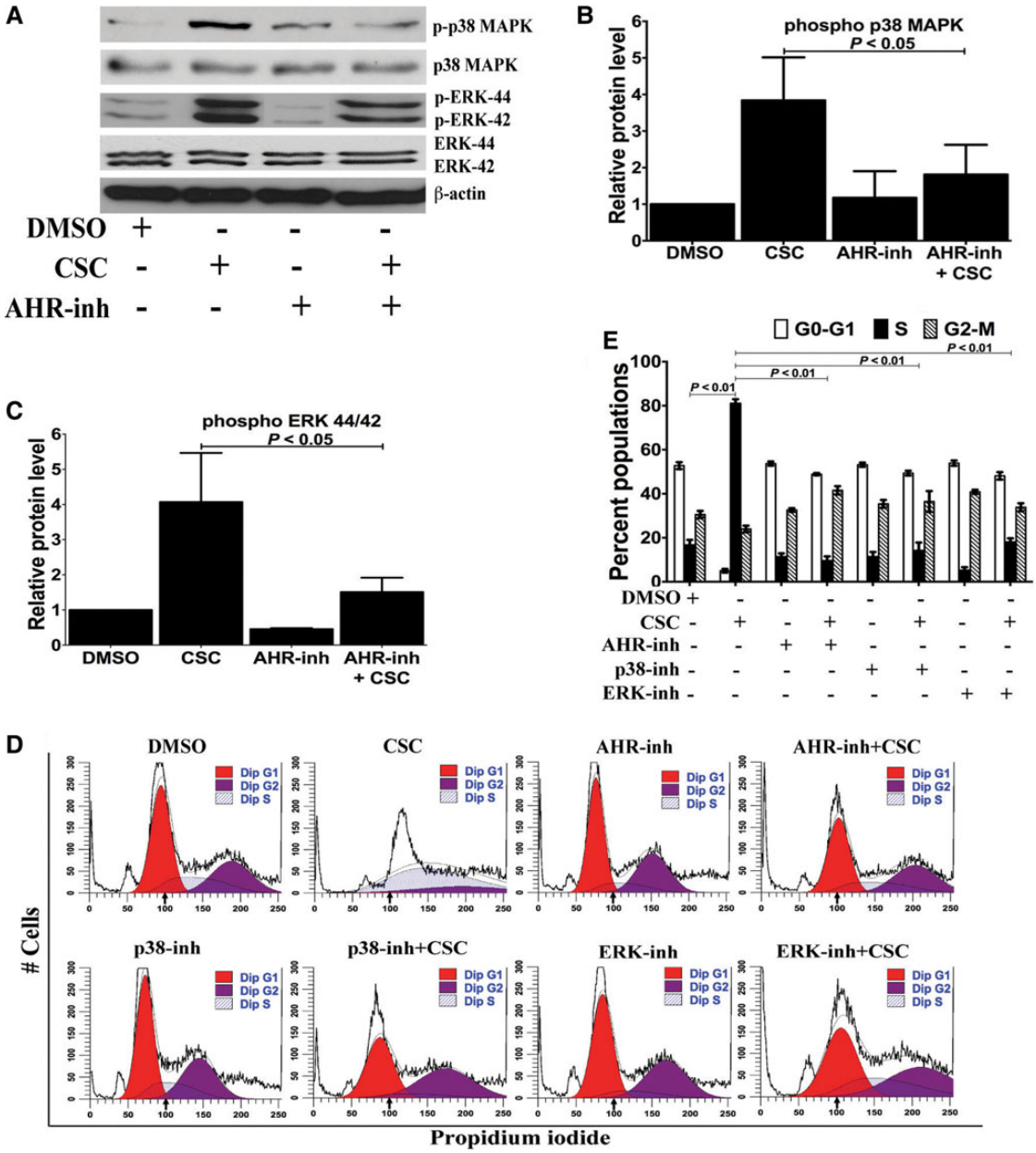

Figure 2 CSC mediates crosstalks between AHR and MAPKs. (**A**) Western blot analysis of GC-2spd(ts) spermatocytes treated with DMSO, CSC (100 μg/ml) for 15 min, AHR-inh (10 μM for 1 h) followed by CSC, or AHR-inh alone. Cell lysates were subjected to SDS–PAGE, probed using anti-phospho-p38 MAPK (Thr180/Tyr182) and anti-phospho ERK-44/42 antibodies, and normalized with anti-p38 MAPK, anti-ERK-44/42, and anti-β-actin antibodies. (**B** and **C**) Histograms represent the activated p38 MAPK (**B**) and ERK-44/42 (**C**) levels in relative densitometric units normalized to β-actin ($n = 3$). (**D**) Pharmacological inhibition rescues cell cycle progress. Spermatocytes were exposed to DMSO (0.1%) or CSC (100 μg/ml) for 24 h. In the antagonists treatment groups, cells were first pretreated with AHR-inh or MAPK-inh for 1 h followed by CSC for 24 h, or treated with inhibitors alone. The percent of cell distribution in G0/G1, S, and G2/M stages was determined by FACS analysis using the BD Modfit LT (V4.0.5) software. The representative histogram demonstrates the stage distribution of spermatocytes at 24 h. Black arrow indicates the population shift. (**E**) Histograms represent the mean ± SEM of flow cytometric data from samples at 24 h of three independent experiments, each assayed in triplicates.

phosphorylates both MAPKs and pretreatment with CH223191 significantly blocks the phosphorylation as evidenced in the densitometric histogram (Figure 2B and C). These data suggest that the CSC constituents activate these MAPKs and the CSC-transformed AHR can regulate MAPK activation.

Pharmacological inhibition mitigates CSC-induced growth arrest

Since CSC activates both AHR and MAPKs, we asked whether blocking the signaling using specific inhibitors could prevent the growth arrest. As shown in Figure 2D and E, CSC treatment causes ~75% ($P < 0.01$) increase in the spermatocyte populations

at S-phase. Pretreatment with AHR-, p38-, and ERK-inh significantly recovered ~45% ($P < 0.01$), ~42% ($P < 0.05$), and ~40% ($P < 0.05$) of CSC-arrested spermatocytes from the S-phase, respectively. These data suggest that CSC-mediated growth arrest of spermatocytes can be overcome by blocking the activation of AHR and MAPKs.

Does siRNA silencing of Ahr–Nrf2 targets mimic CSC-induced growth arrest?

Since the CSC-induced signaling has led to growth arrest, we wanted to determine whether the MAPKs-mediated *Ahr–Nrf2* targets directly involved in spermatocyte cell cycle through siRNA silencing. As shown in Figure 3, flow cytometry revealed that the suppression of *Ahr* and its downstream *Nrf2* caused significant increase ($P < 0.05$) in G2-M-phase spermatocytes (Figure 3A and B) while the stress-inducible *Atf3* and *E2f4* gene silencing caused significant increase ($P < 0.05$) at S-phase (Figure 3C and D). These data directly implicate the *Ahr–Nrf2* pathway and other candidate genes in cell cycle progression, which reflect the growth inhibitory nature of CSC.

Do the CSC-activated MAPKs regulate AHR target genes?

Based on p38 and ERK MAPK activation, we decided to determine whether the CSC-activated and AHR-mediated MAPKs regulate antioxidant and growth suppressive genes of AHR pathway. We exposed spermatocytes to CSC and determined the expression of master regulator of oxidative stress and stress-inducible and growth inhibitory *Nrf2* and *Atf3* genes in presence or absence of inhibitors. As seen in Figure 4A, qRT-PCR demonstrated that the transcript levels of *Nrf2* (~5-fold) and *Atf3* (~20-fold) were significantly elevated in CSC-treated cells. Pretreatment with AHR-inh and p38-inh has significantly blocked the CSC-induced *Nrf2* mRNA ($P < 0.05$) but not *Atf3* ($P < 0.06$) (Figure 4A and B). However, ERK-inh significantly abrogated the CSC induction of *Nrf2* and *Atf3* (Figure 4C). Western blot (Figure 4D) shows that CSC exposure causes significant elevation of both NRF2 and ATF3. Pretreatment with inhibitors blocked the CSC-induced increase in NRF2; however, CSC induction of ATF3 seemed to be reversed by ERK-inh alone as supported by densitometry (Figure 4E and F). There was no change in the expression of the spermatocyte-specific HSPA2 across the treatment groups. Taken together, these data clearly indicate that the CSC-induced NRF2 was regulated by both AHR and MAPKs whereas ATF3 appears to be under ERK MAPK.

Does CSC activate NRF2, and ATF3 proteins via p38 and ERK MAPKs?

After establishing the crosstalks between AHR and the MAPKs, we interrogated whether the CSC-induced MAPKs also activate the candidate transcription factors of AHR pathway. CSC causes nuclear translocation of NRF2 and preincubation of spermatocytes with ERK-inh (Figure 5A) and p38-inh (Figure 5B) almost blocked the nuclear import of NRF2. Histograms (Figure 5C and D) represent the mean nuclear cytoplasmic ratio of NRF2-positive fluorescence. Similarly, the nuclear signal for ATF3 increased significantly by 2 h of CSC exposure and ERK-inh (Figure 5E) but not p38-inh (Figure 5G) inhibited ATF3 nuclear shuttling as represented by its respective histograms (Figure 5F and H). These data suggest the regulation of activation and intracellular localization of NRF2 and ATF3 proteins by CSC-induced p38 and ERK MAPKs in spermatocytes.

Atf3 is downstream to Nrf2 in CSC-induced spermatocytes

Our previous study demonstrated that spermatocytes elevate *Nrf2* in response to CSC and the crosstalk between *Nrf2* and *Ahr* (Esakky et al., 2014). Given that the CSC induces *Nrf2* and several

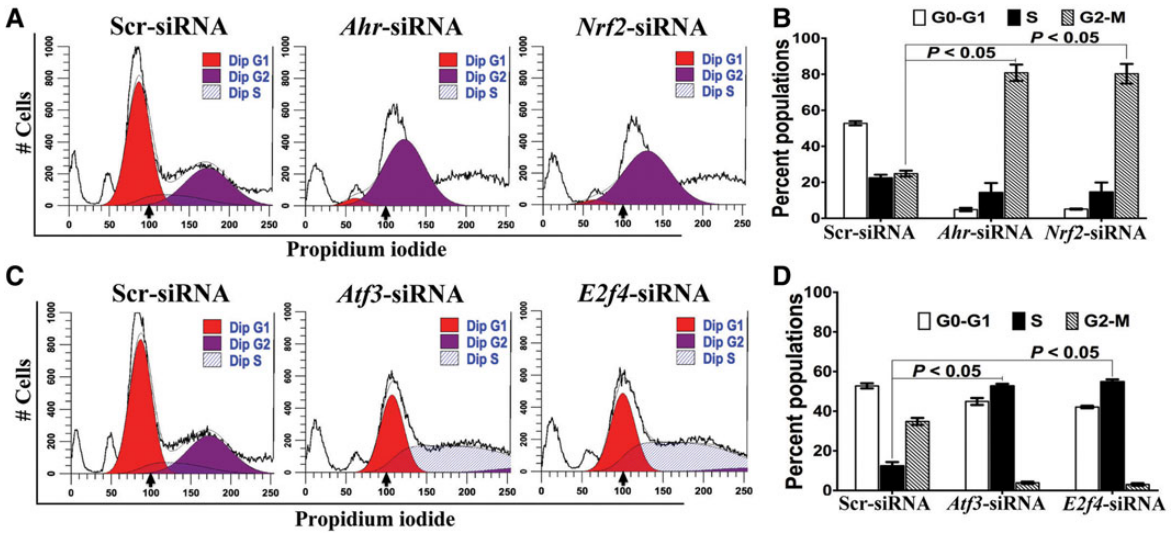

Figure 3 SiRNA silencing of *Ahr–Nrf2* targets interrupts cell cycle. Spermatocytes were transfected individually with Scr, *Ahr*, *Nrf2* (**A** and **B**), *Atf3*, and *E2f4* (**C** and **D**) siRNAs. Phase distribution of the transfected spermatocytes stained with propidium iodide was FACS analyzed using the BD Modfit LT (V4.0.5) software. Black arrow indicates the population shift. Histograms (**B** and **D**) display the mean ± SEM of flow cytometric data from respective siRNA-knockdown groups ($n = 3$).

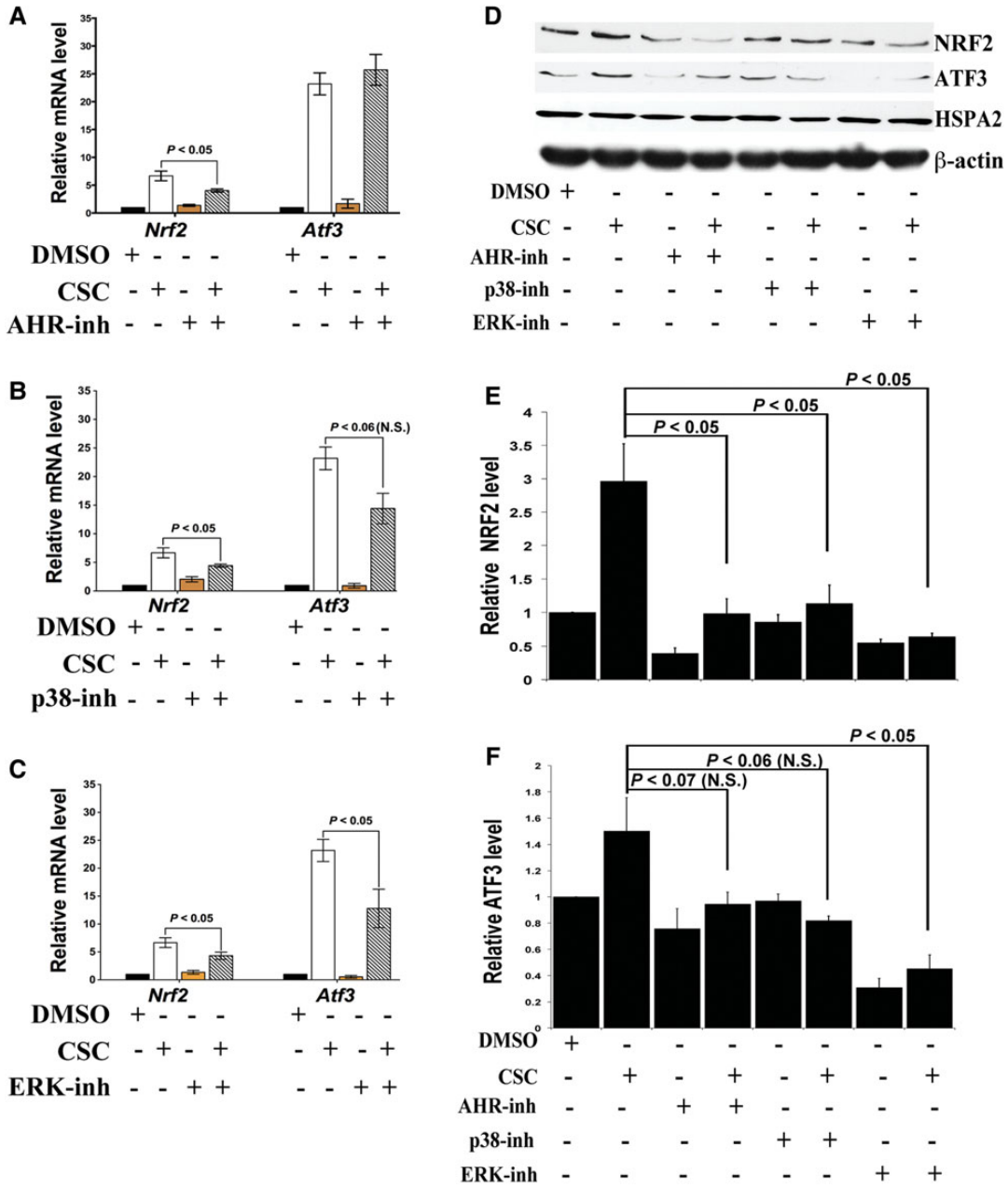

Figure 4 CSC-activated MAPKs regulate *Nrf2* and *Atf3*. The mRNA levels of *Nrf2* and *Atf3* in GC-2spd(ts) spermatocytes, treated with DMSO (0.1% for 6 h), CSC (100 μg/ml for 6 h), CSC plus AHR-inh (**A**), CSC plus p38-inh (**B**), CSC plus ERK-inh (**C**), and AHR-inh (10 μM for 1 h), p38-inh (10 μM for 1 h), or ERK-inh (25 μM for 1 h) alone, were determined by qRT-PCR. Data are expressed as the mean ± SEM of four independent experiments assayed in duplicates. $P < 0.05$. (**D**) Western blot analysis of GC-2spd(ts) cells treated with DMSO, CSC, CSC plus AHR or MAPK antagonists, and antagonists alone. Cell lysates were subjected to SDS–PAGE, probed using anti-NRF2, anti-ATF3, and anti-HSPA2 antibodies, and reprobed with anti-β-actin for normalization. (**E** and **F**) Histograms represent NRF2 (**E**) and ATF3 (**F**) levels in relative densitometric units normalized to β-actin ($n = 3$).

of its downstream antioxidants, we sought to determine whether CSC could regulate *Atf3*, via *Nrf2*. SiRNA silencing of *Nrf2* caused significant downregulation of both *Nrf2* and *Atf3* at mRNA (Figure 6A and B) and protein levels (Figure 6D and E) in presence or absence of CSC. Similarly, the siRNA knockdown of *Ahr* significantly if not completely, prevented the CSC induction of *Atf3* at mRNA and protein levels (Figure 6C and F). These data indicate that the CSC-induced *Nrf2* and *Atf3* might be under a similar regulatory pathway based on their interlink and *Nrf2* could be a direct upstream mediator of *Atf3* in spermatocytes.

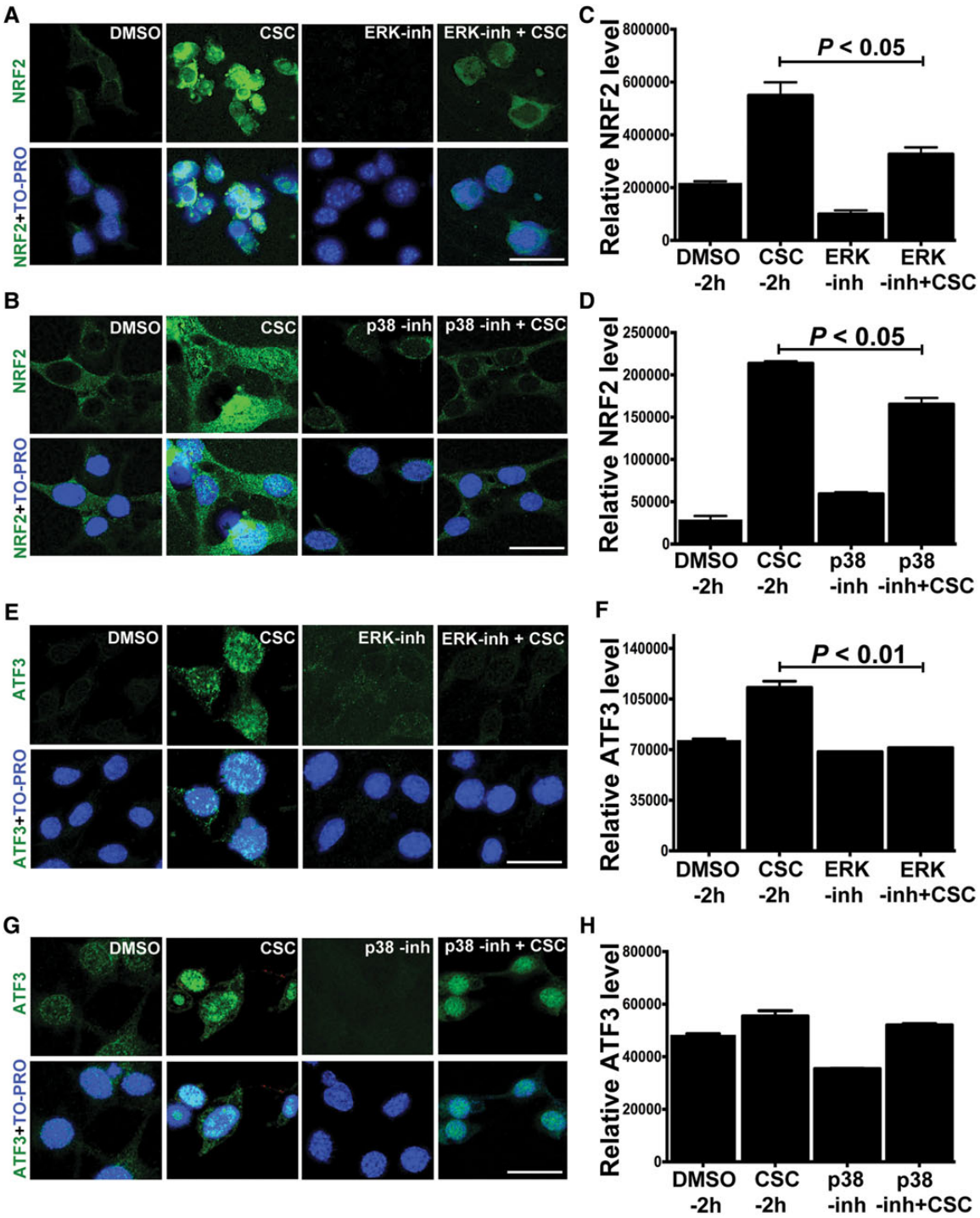

Figure 5 CSC-mediated nuclear translocation of NRF2 and ATF3 proteins is regulated by p38 and ERK MAPKs. Spermatocytes grown on chamber slides were exposed to DMSO, CSC, antagonists followed by CSC, or the antagonists alone. Cells were immunolocalized with anti-NRF2 (**A** and **B**) and anti-ATF3 (**E** and **G**) antibodies. Merged panel represents the immunosignal for NRF2 and nuclear counterstain, TO-PRO-3 iodide. A minimum of 50 cells of each group was imaged with identical exposure conditions. Scale bar, 50 μm. Histograms represent the mean nuclear/cytoplasmic ratio of the NRF2- or ATF3-specific fluorescence (**C** and **D** for NRF2; **F** and **H** for ATF3) analyzed by Image J.

Does CSC-induced Atf3 alter growth-modifying E2F4 in spermatocytes?

CSC treatment causes oxidative stress and cell death in spermatocytes (Esakky et al., 2012, 2014). To understand the mechanistic effects of CSC on spermatocyte growth arrest, we examined the growth-repressive *E2f4* and its possible regulation by *Atf3* post CSC exposure. As seen in Figure 7A and B, qRT-PCR of CSC-exposed spermatocytes demonstrated a higher level ($P <$

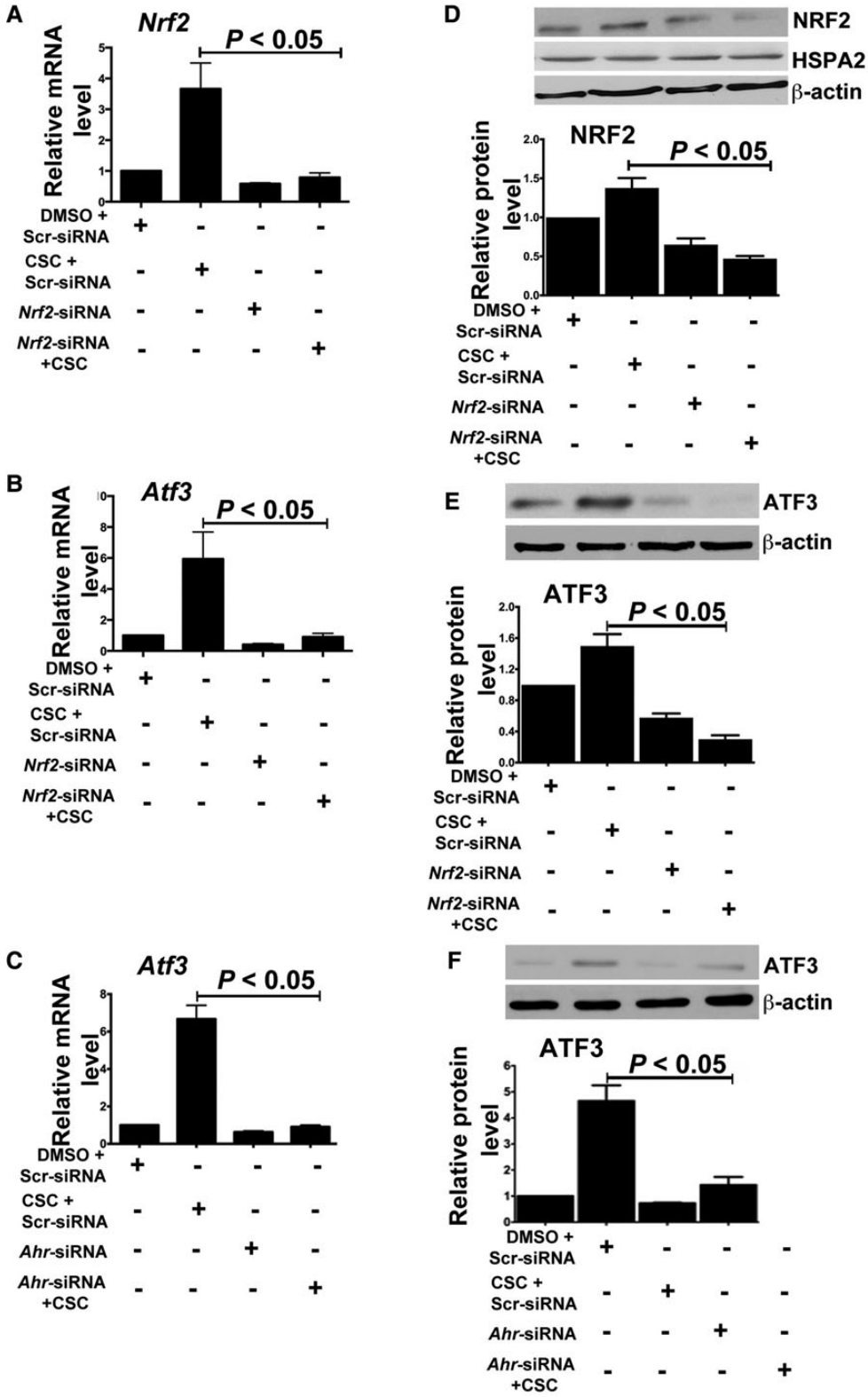

Figure 6 *Nrf2* is upstream to *Atf3* in CSC-exposed spermatocytes. Spermatocytes were transfected with scrambled (Scr), *Nrf2*, and *Ahr* siRNAs and treated with or without CSC. QRT-PCR was performed to assess *Nrf2* and *Atf3* expression and the histogram reflects the relative fold difference in *Nrf2* (**A**) and *Atf3* (**B** and **C**) expressions. Western blot analysis was performed to determine NRF2, HSPA2 (**D**), and ATF3 (**E** and **F**) expression. Histograms represent NRF2 and ATF3 protein levels in relative densitometric units normalized to β-actin ($n = 3$).

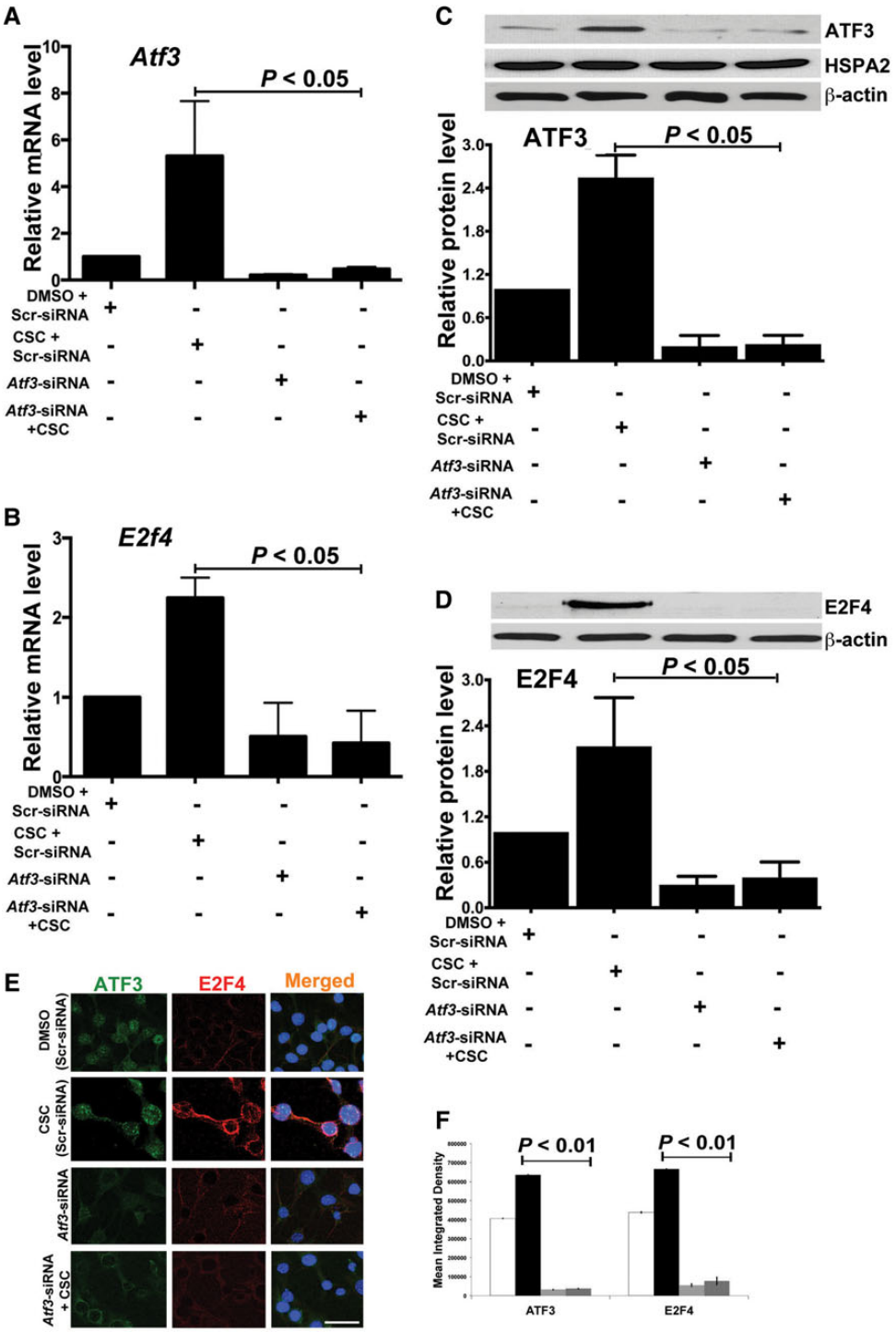

Figure 7 CSC-stimulated E2F4 expression is mediated by ATF3. Spermatocytes were transfected with Scr-siRNA or *Atf3*-siRNA and treated with or without CSC. (**A** and **B**) QRT-PCR was performed to assess the expression of *Atf3* and *E2f4*. The histogram reflects the relative fold difference in *Atf3* and *E2f4* expressions. (**C** and **D**) Western blot analysis was performed to determine ATF3, HSPA2 (**C**) and E2F4 (**D**) expression. Histograms represent the ATF3 and E2F4 protein levels in relative densitometric units normalized to β-actin ($n = 3$). (**E**) Immunofluorescent colocalization of ATF3 and E2F4 proteins with TO-PRO-3 iodide for nuclear stain. (**F**) The histogram represents the mean fluorescence integrated density of ATF3 and E2F4 ($n = 3$). A minimum of 50 cells of each group were imaged with identical exposure conditions. Scale bar, 50 μm. White bar, DMSO + Scr-siRNA; Black bar, CSC + Scr-siRNA; Horizontal line bar, *Atf3*-siRNA; Diagonal line bar, CSC + *Atf3*-siRNA.

0.05) of *Atf3* and *E2f4* transcripts. Spermatocytes transfected with *Atf3*-siRNA showed decrease in the levels of both *Atf3* (Figure 7C) and *E2f4* (Figure 7D) transcripts and CSC could not enhance their expressions.

Immunolocalization showed that the E2F4-specific signal was more pronounced in the cytoplasm of CSC-exposed while completely reduced in the *Atf3*-silenced or *Atf3*-silenced plus CSC-exposed spermatocytes. ATF3 found disappeared in the transfected and CSC-exposed spermatocytes (Figure 7E and F). However, the *Nrf2* or *Atf3* silencing had no off-target effects on *Hspa2* or β-*actin* and *Gapdh* genes (data not shown), confirming the siRNAs' specificities. This finding suggesting CSC-induced ATF3 and its translocation might in turn regulate E2F4 function in the spermatocytes.

CSC-mediated E2F4 undergoes regulation of multiple signaling

To determine whether the CSC-induced E2F4 follows similar pharmacological regulation, we evaluated its expression in presence of AHR and MAPKs inhibitors followed by CSC exposure. The antagonists attenuated the CSC induction of *E2f4* transcripts (Figure 8A) with significant downregulation by ERK-inh at protein level (Figure 8B). Coincidently, pretreatment with either p38-inh (Figure 8C and D) or ERK-inh (Figure 8E and F) significantly weakened the E2F4-specific immunosignal post-CSC exposure. In order to estimate the percent of spermatocytes expressing CSC-stimulated E2F4 following pharmacological inhibition, we performed flow cytometry to determine the generation of $E2F4^+$ (E2F4-positive) populations. As seen in Figure 8G and H, CSC significantly enhanced $E2F4^+$ spermatocytes (∼40%) compared with DMSO (∼4%). Treatment with AHR-inh (0.7%), p38-inh (2.0%), and ERK-inh (1.7%) alone did not significantly alter the basal E2F4 expression. However, pretreatment with antagonists to AHR (∼2.2%), p38 MAPK (∼10%), and ERK MAPK (∼7%) noticeably reduced the generation of CSC-induced $E2F4^+$ spermatocytes. The significant decrease in CSC-stimulated $E2F4^+$ spermatocytes by pharmacological inhibition suggests that multiple metabolic pathways are interlinked in the regulation of E2F4 expression by spermatocytes.

Discussion

The present study demonstrates that the growth inhibitory effect of cigarette smoke condensate (CSC) on spermatocytes involves a bidirectional crosstalk between AHR and MAPK pathways and regulation of a cascade of downstream target genes. CSC treatment to the spermatocyte *in vitro* causes AHR-dependent activation of p38 and ERK MAPKs, which in turn regulates the *Ahr*-target of *Nrf2*; stress-inducible *Atf3*, and growth-suppressive *E2f4* genes. Pharmacological inactivation of AHR and MAPKs rescued the CSC-induced growth-arrested spermatocytes. SiRNA silencing of *Ahr–Nrf2* targets reveals their direct involvement in spermatocyte cell cycle, and in some cases mimics CSC-induced growth inhibition. Based on this, we have proposed a model (Figure 9), which illustrates the interrelationship between the pathways that might have led to the growth arrest.

Cigarette smoke causes growth arrest followed by cell death in spermatocytes (Esakky et al., 2014) and other cell types (Fields et al., 2005). Measurement of incorporation of thymidine analogs such as bromodeoxyuridine and EdU into DNA is the 'gold standard' method of determining cell proliferation (Gratzner, 1982; Salic and Mitchison, 2008). As depicted here, the significant accumulation of EdU-negative CSC-exposed spermatocytes during S-phase accompanied with downregulation of cyclins A and E exemplifies our earlier notion that the CSC causes S-phase arrest by blocking DNA synthesis and subsequent cell cycle progress. These data corroborate a similar report demonstrating TCDD effect on mouse epithelial cells (Gierthy and Crane, 1984).

Since the CSC-mediated S-phase accumulation is most likely through AHR and MAPKs, we intend to identify specific CSC-responsive MAPKs in spermatocytes. We demonstrated here that the CSC activates p38 and ERK MAPKs through AHR and pharmacological inhibition of these pathways significantly rescued cell cycle progress. Once establishing the CSC-induced signaling in growth-arrested spermatocytes, we examined the direct influence of MAPKs-mediated *Ahr–Nrf2* targets in cell cycle by siRNA silencing. Several studies explored the role of AHR in cell cycle regulation; however, the precise mechanism remains cryptic (Ma and Whitlock, 1996; Weiss et al., 1996). In this study, the G2-M accumulation of *Ahr*- and *Nrf2*-silenced spermatocytes correlates with earlier studies wherein the *Ahr* and *Nrf2* loss altered G2/M kinase expression (Elizondo et al., 2000) and induced DNA lesions (Reddy et al., 2008), respectively. Meanwhile, the *Atf3* and *E2f4* suppression simulated the CSC-mediated S-phase arrest as previously reported (Lu et al., 2006; Garneau et al., 2009). Therefore, the loss of gene function data indicates that the candidate genes play an important endogenous role during spermatocyte cell cycle and the molecular response of spermatocytes varies significantly depending upon the nature of cellular stimuli.

The most potent AHR-ligand, TCDD regulates ERK indirectly (Patel et al., 2006) and reduction in AHR amount strongly diminished TCDD-enhanced p38 phosphorylation (Weiss et al., 2005). Given that the functional dependency of MAPKs on AHR is cell type-specific, the MAPK activation in spermatocytes suggests that the CSC constituents that activate p38 and ERK MAPKs might also be the ligands of AHR. If this were the case, inhibition of MAPK activity would prevent AHR activation and resultant-dependent gene expression. Earlier studies based on TCDD-mediated MAPK regulation indicated the role of MAPK in AHR activation (Tan et al., 2002). Even though AHR-inh and p38-inh have exhibited the desired mitigative effect on CSC as demonstrated here, previous studies using this p38-inh appear to be enigmatic (Korashy et al., 2011). *Atf3* regulation by MAPK correlates with previous reports indicating the role of ERK and p38 MAPKs (Lu et al., 2007). However, its incomplete inhibition by AHR- and p38-inh reiterates higher complexity of the cigarette smoke and hyperinducibility of this early response gene. Meanwhile, the triple inhibition of AHR, ERK, and p38 MAPK pathways caused nearly complete suppression of CSC-induced *Nrf2, Atf3,* and *E2f4* (data not shown). It suggests that the complete AHR activation is likely to involve multiple MAPK signaling.

Atf3 has been known to be induced by the CSC constituent, benzo(a)pyrene diol epoxide (Hai et al., 1999). Having established the

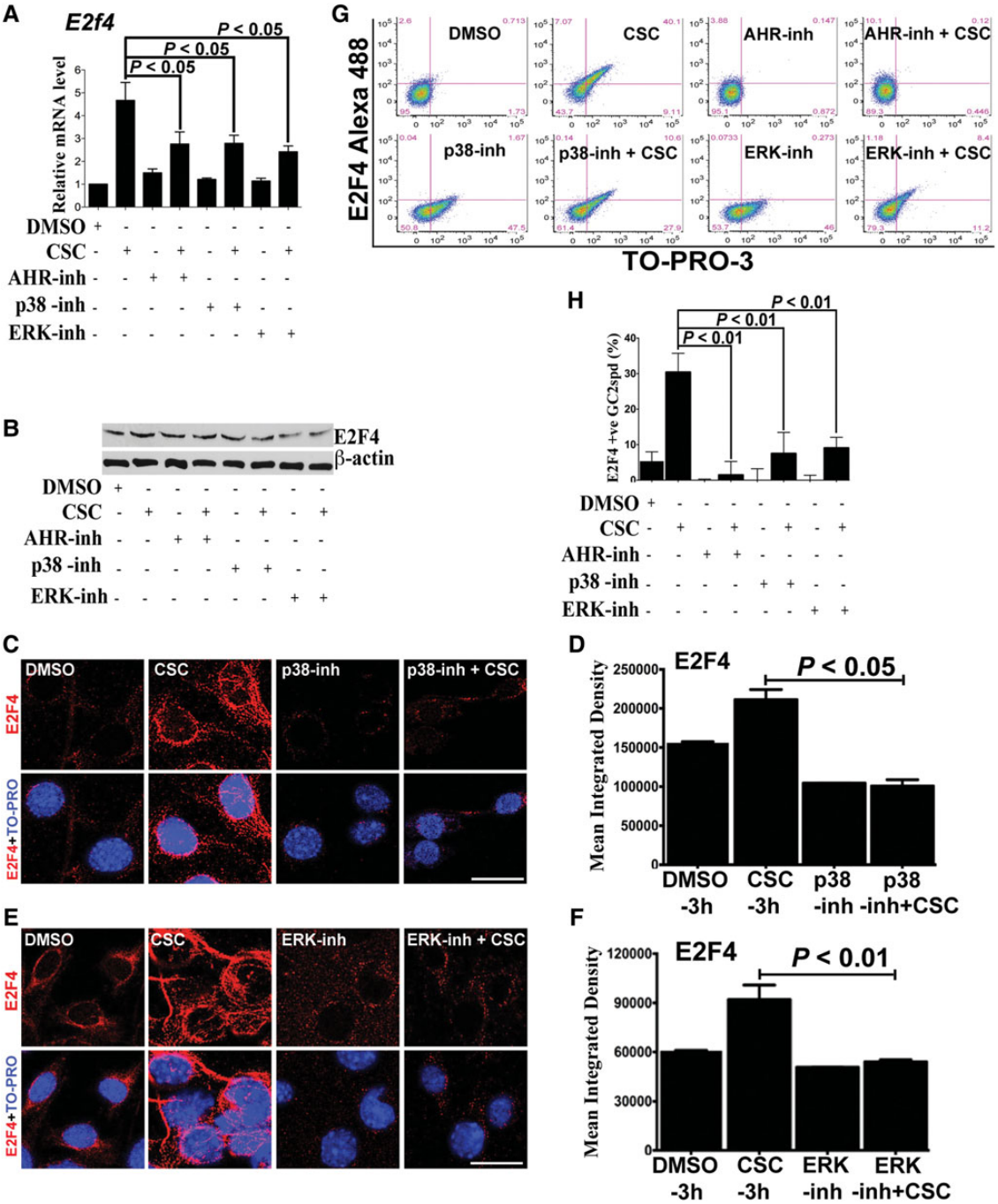

Figure 8 CSC-mediated E2F4 undergoes multiple regulations. Spermatocytes exposed to DMSO, CSC, or inhibitors as detailed in Figure 4 were analyzed to determine the changes in *E2f4* mRNA level by qRT-PCR (**A**), E2F4 protein level by western blot (**B**), and its localization by immunofluorescence (**C** and **E**). A minimum of 50 cells of each group were imaged with identical exposure conditions. (**D** and **F**) Histograms represent mean fluorescent integrated density of E2F4 protein ($n = 3$). Scale bar, 50 μm. (**G**) Flow cytometric evaluation of CSC-induced E2F4^{+} spermatocytes. Spermatocytes were treated with CSC and inhibitors followed by immunolocalization using anti-E2F4 and TO-PRO-3 iodide. E2F4 expression was assessed after 24 h of exposure to CSC or CSC plus antagonists. Dot plots with quadrant markers show two-parameter analysis of fluorescein intensity of E2F4 (BluFL1 on *Y*-axis) and TO-PRO-3 (RedFL1 on *X*-axis) among treated spermatocytes. Data depict a representative result of four separate experiments and the percent difference in the generation of E2F4^{+} cells. Bottom left quadrant = low E2F4 and normal TO-PRO-3 staining, bottom right quadrant = high TO-PRO-3 staining, top left quadrant = high E2F4 staining, and top right quadrant = high E2F4 and normal TO-PRO-3 staining. Percentages of cells in each quadrant are indicated. (**H**) The histogram represents the mean flow cytometric data of each group from four independent experiments ($n = 4$).

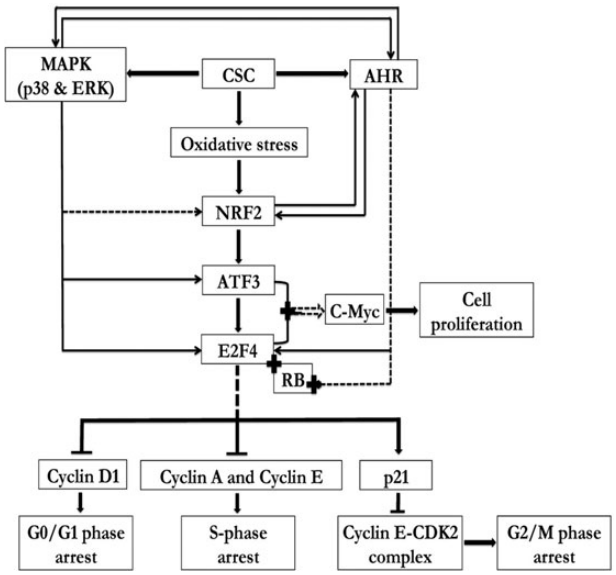

Figure 9 Proposed model of CSC-mediated molecular signaling and regulation of their potential targets in spermatocytes. CSC activates p38 and ERK MAPKs in a temporal fashion either directly or indirectly through activated AHR. CSC by itself or the CSC-activated MAPKs in turn regulates potential targets of *Ahr–Nrf2* pathway such as *Atf3*. Other stress-related pathways induced by oxidative imbalance can also modulate the stress-inducible *Nrf2*-regulated *Atf3*. CSC induction of *Atf3* in spermatocytes possibly elicits growth-arresting response by invoking the expression of the *E2f4* transcription factor toward growth repression. Once induced, the CSC-mediated E2F4 undergoes regulation by crosstalking multiple molecular signaling as shown here while regulating several of its downstream targets associated to DNA synthesis and repair, cell cycle such as *Ccnd1, Cyclin A, Cyclin E,* and maintaining the level of cell cycle inhibitors such as *p21*. Stimulation of a cascade of downstream targets following activation and crosstalks between AHR–NRF2 and MAPK pathways illustrates the existence of a complex network of cell signaling behind the CSC-mediated growth inhibition of spermatocytes. Discontinuous lines indicate published studies (Ge and Elferink, 1998; Puga et al., 2000; Garneau et al., 2009; Jeong et al., 2010).

CSC-mediated *Ahr–Nrf2* crosstalk (Esakky et al., 2014), we set out to determine whether CSC mediates similar crossinteraction between *Nrf2* and *Atf3* based on their regulation by ERK MAPK and the presence of antioxidant response elements (AREs) (Kim et al., 2010) in the *Atf3* promoter. As shown here, the siRNA knockdown of *Nrf2* and *Ahr* downregulates *Atf3* and CSC did not reverse that. However, its incomplete inhibition by *Ahr* silencing could be attributed to partial suppression of *Ahr* and/or the absence of AHR response elements in the *Atf3* promoter. The paradox in *Atf3* regulation by the closely associated *Ahr–Nrf2* pathway in spermatocytes indicates the interplay of other upstream regulators induced by oxidative stress, which mediates the expression of *Nrf2*.

In order to elucidate further the possible mechanism behind this growth arrest, we studied the molecular response of E2F4 to CSC for the following reasons. First, E2F4 accounts for the majority of endogenous E2F species with subcellular transcriptional regulation (Lindeman et al., 1997). Second, *E2f4* regulates genes required for S-phase progress, DNA synthesis, and repair (Ren et al., 2002). Third, *E2f4* silencing impedes G1/S phase transition, causes S-phase arrest and downregulates cyclins in spermatocytes as shown in the present study, and upregulates cell cycle inhibitors p21 and p27 (Garneau et al., 2009). Our finding of the significant E2F4 elevation by CSC corroborates a previous report that shows *E2f4* as a coregulator of *Egr-1* in cigarette smoke-induced autophagy (Chen et al., 2008).

The transcriptional silencing of *Atf3* in accordance with an earlier study (Janz et al., 2006) blunted CSC-induced *E2f4* expression and site-specific localization. Since CSC accumulates E2F4 in the cytoplasm of spermatocytes and the activated ATF3 has been reported earlier in a nuclear complex of SMAD3 and E2F4 (Massague et al., 2005), we believe that the CSC-activated ATF3 might act as a scaffolding protein responsible for nuclear export of E2F4. On the other hand, the alteration in the relative levels of nuclear and cytoplasmic E2F4 could be caused by either the translocation of preexisting E2F4 or the combined effect of degradation of nuclear E2F4 and the *de novo* synthesis of cytoplasmic protein by CSC. However, further studies are warranted to unravel the link if any between nuclear import and export of ATF3 and E2F4 proteins, respectively. Given that *Atf3* is the upstream mediator of *E2f4*, the discrepancy in p38 regulation of ATF3 and E2F4 proteins indicates the participation of additional molecules such as AHR.

Since the transcriptional activity of nuclear *E2f4* is markedly high (Deschênes et al., 2004), CSC induction of E2F4 was expected to augment proliferation of spermatocytes, although the CSC treatment resulted in S-phase arrest accompanied with downregulation of *Ccnd1, Cyclin A*, and *Cyclin E*. Our previous studies have reported the CSC-induced *p21* expression and AHR activation in spermatocytes (Esakky et al., 2012, 2014). Several cell lines of evidence suggest that the ligands of CSC such as TCDD have contributed toward cell cycle arrest (Ge and Elferink, 1998; Barnes-Ellerbe et al., 2004) by mediating a direct interaction between the transformed AHR and the retinoblastoma (RB)/E2F axis. Based on this, we propose in the current model of E2F4 action that the CSC-induced E2F4 forms a triad of inhibitory complex, AHR-RB-E2F4 via activated AHR and hypophosphorylated RB (most probably p130, Deschênes et al., 2004). This repressive complex might directly inhibit E2F4-dependent target genes such as cyclins as observed in the present study or prevent E2F4 from promoting their expression by 'molecular trapping' by the AHR-bound RB protein or simply due to its nuclear exclusion mediated by *Atf3*. Therefore, it necessitates the need to explore the above possibilities in order to understand the downstream regulation of E2F4 in cigarette smoke-exposed cell types.

Given that the CSC elicits complex intracellular signaling *in vitro*, our data are of particular interest and attain greater significance because of its conformity to an *in vivo* study involving TCDD-mediated MAPK signaling in mouse testis (Jin et al., 2008) and suggesting explicitly that each pathway is interlinked and unique in AHR activity. The data also reveal the ability of spermatocytes to deal with different kinds of cellular stimuli via activation of specific signaling pathways during growth. The resumption of

spermatocyte cell cycle through pharmacological inactivation of CSC-induced AHR and MAPKs indicates interconnect among the signaling network. Therefore, the delineation of CSC-activated *de novo* pathways, uncovering their interactions and regulation of their downstream targets as demonstrated in this study will shed further light on the molecular mechanisms of CSC-induced cellular toxicity.

Materials and methods

Cell culture and in vitro CSC and antagonists treatment

Cigarette smoke condensate (CSC) (40-mg/ml in 100% DMSO) purchased from Murty Pharmaceuticals, Inc. was prepared as reported earlier (Esakky et al., 2012). The mouse spermatocyte cell line GC-2spd(ts) (ATCC) (Wolkowicz et al., 1996), hereafter referred to as spermatocytes was treated with a previously optimized concentration of CSC at 100 μg/ml (Esakky et al., 2012) and 10 μM AHR-specific antagonist, CH223191 (2-Methyl-2H-pyrazole-3-carboxylic acid-(2-methyl-4-o-tolyl-azophenyl)-amide) (EMD chemicals) (Kim et al., 2006). To evaluate CSC-activated MAPKs in AHR function, MAPK inhibitors such as SB203580 (SB) (p38 MAPK; Rutault et al., 2001) and PD98059 (PD) (ERK MAPK/MEK1 inhibitor; Dudley et al., 1995) were used. GC-2spd(ts) grown to 70% confluence were serum starved for 24 h. The growth-synchronized cells were treated with CSC for different time durations to determine gene expressions at mRNA and protein levels by qRT-PCR and western blot, respectively.

RNA isolation, cDNA synthesis, and qRT-PCR

Following incubation, the total RNA from treated cells was isolated using Trizol reagent (GIBCO BRL) and used for cDNA synthesis and qRT-PCR as previously reported (Esakky et al., 2013). QRT-PCR was performed based on relative quantification by using TaqMan gene expression assays (Applied Biosystems) with the ABI 7500 FAST (Applied Biosystems) as per MIQE guidelines (Bustin et al., 2009). The $2^{-\Delta\Delta CT}$ method (Livak and Schmittgen, 2001) employed to analyze gene expression reflects the relative fold difference between the control and treated groups among candidate genes.

EdU (5-ethynyl-2′-deoxyuridine) incorporation and Click-iT assay

To determine whether CSC induces S-phase arrest by inhibiting DNA synthesis, we performed a nonradioactive EdU-based assay by using a Click-iT EdU flow cytometry assay kit (Molecular Probes). EdU, the thymidine nucleoside analog is incorporated into DNA during active DNA synthesis (Salic and Mitchison, 2008). In brief, the serum-starved spermatocytes (1×10^6/ml) were treated with DMSO or CSC (100 μg/ml) for 24 h in presence of EdU (10 μM) in DMEM containing 10% FBS. The harvested cells were fixed with 4% paraformaldehyde and permeabilized using ice-cold 100% ethanol for 1 h. Followed by washing in 1% BSA-PBS wash solution, the click reaction was carried out using a Click-iT reaction mix containing Alexa Fluor 488 azide as per the manufacturer's protocol. EdU incorporation into DNA detected by the azide-tagged Alexa Fluor 488 dye was evaluated by using a FACScalibur flow cytometer (Becton-Dickinson) and the data were analyzed using the BD Modfit LT (V4.0.5) software.

CSC activation and AHR regulation of MAPK

To determine whether cigarette smoke causes activation of p38 and ERK MAPK signaling *in vitro* via AHR, the GC-2spd(ts) cells were treated separately with DMSO (0.1%), CSC (100 μg/ml for 15 min), CSC + CH223191 (AHR-inh), or CH223191 (10 μM for 1 h) alone and subjected to western blot analysis.

CSC-activated MAPK regulation of AHR target genes

Spermatocytes were treated separately to DMSO (0.1% for 6 h), CSC (100 μg/ml for 6 h), CSC + CH223191 (AHR-inh), CSC + PD98059 (ERK-inh), CSC + SB203580 (p38-inh), and CH223191 (10 μM)/PD98059 (25 μM)/SB203580 (10 μM) alone for 1 h. Following incubation, total RNA isolated from the treated cells was used for cDNA synthesis, and qRT-PCR was employed to determine *Nrf2*, *Atf3*, and *E2f4* expression in the exposed spermatocytes (Esakky et al., 2013). Spermatocytes pretreated with inhibitors as described above followed by CSC for 24 h were harvested in RIPA buffer [0.1 M PMSF (Sigma-Aldrich), 1 mM EDTA, 1 mM sodium orthovanadate, 1 mM sodium fluoride, and 1× mini protease inhibitor cocktail (Roche Applied Science)], and subjected to western blot analysis. For immunofluorescence, the spermatocytes cultured on a 4-chambered slide (Nalge Nunc) were treated with CSC for 2 h and inhibitors as detailed above, and localized using antibodies to NRF2, ATF3, and E2F4.

Cell cycle analysis by flow cytometry

Spermatocytes (1×10^6/ml) exposed to CSC (100 μg/ml) for 24 h and various inhibitors as detailed above were analyzed by flow cytometry for cell cycle progression using our previously established protocol (Esakky et al., 2014). DNA content of the phases was measured by using a FACScalibur flow cytometer (Becton-Dickinson) and BD Modfit LT (V4.0.5) software was used to analyze the percentages of cells in G0/G1, S, and G2/M phases as suggested by the reviewers.

Determination of CSC-mediated E2F4 regulation

To understand how the CSC exposure and pharmacological inhibition of pathways in spermatocytes alter E2F4 expression, we performed intracellular immunostaining as per the Cell Signaling Technology protocol and others (Krutzik et al., 2005) with a slight modification, and analyzed E2F4 expression by flow cytometry using a FACScalibur flow cytometer (Becton-Dickinson). In brief, following 24 h of CSC induction or pretreatment with inhibitors as described above, cell suspensions ($n = 3$) were fixed in 1.5% PFA for 10 min at RT, permeabilized using ice-cold methanol for 10 min at 4°C followed by blocking in 0.5% BSA-PBS blocking buffer for 15 min at RT. The cells stained with mouse anti-E2F4 (Santa Cruz; dilution 1:50) for 30 min at RT were washed twice in blocking buffer, and incubated in Alexa Fluor 488-conjugated goat anti-mouse secondary antibody (dilution 1:2000) along with the nuclear dye, TO-PRO-3 iodide (Molecular Probes) for 30 min at RT. Mouse immunoglobulin G1 (IgG2a) (Sigma-Aldrich) isotype control at equal concentration served as negative control. Following staining, the cells were washed and resuspended in 0.5 ml of 1× PBS for analysis.

Flow cytometric analysis

Different groups of treated cells were evaluated for E2F4-positive ($E2F4^+$) populations based on compensation calculations on BD FACSCalibur using FlowJo software (v9.7.5). To analyze E2F4 expression, a gate was first drawn around the single cell populations in a dot plot of forward scatter versus BLFL1 (E2F4). A dot plot of E2F4 ($BLFL1^+$) versus TO-PRO-3 iodide (RedFL1) was drawn based on the subclass control and the quadrant markers were set according to both the unstimulated control and the isotype control. The percentage of $E2F4^+$ spermatocyte subsets was computed using the following formula based on the percentage of gated values given for the $BLuFL1^+$ cells: (stimulated − stimulated isotype control) − (unstimulated − unstimulated isotype control). Markers used to assess a shift in fluorescence of the proteins were set based on the unstimulated (control) cultures.

SiRNA transfection and CSC treatment

SiRNA transfection was carried out based on our established protocol (Esakky et al., 2014) and earlier studies (Abdelrahim et al., 2003). Spermatocytes grown in 6-well or 100 mm plates were allowed to transfect for overnight by siRNAs (final concentration of 140 nM) to *Ahr*, *Nrf2*, *Atf3*, and *E2f4* genes or scrambled (Scr) siRNAs (Ambion) alone in DMEM without growth factors and antibiotics. DMEM with 10% FBS was used to evaluate cell cycle progression by flow cytometry. To determine the direct impact of siRNA silencing of the candidate genes on spermatocyte growth, the DNA content of various groups of siRNA-transfected populations at G0/G1, S, and G2/M was measured by using a FACScalibur flow cytometer (Becton-Dickinson), and analyzed by the BD Modfit LT (V4.0.5) software as described earlier. The transfected spermatocytes were treated with CSC for 6 h for RNA isolation and 24 h for western blot. For immunofluorescence, the transfected and CSC-treated cells were immunolocalized with antibody to ATF3 and E2F4. Each transfection assay was repeated a minimum of three times, and the results are shown as the mean ± SEM of independent experiments.

Western blot analysis

Following CSC treatments, cells were washed with ice-cold PBS and scraped into RIPA buffer. Aliquots of 40 μg of protein from transfected and CSC-treated cells were separated by SDS–PAGE and electroblotted onto nitrocellulose membrane. The blots were probed with rabbit anti-NRF2, anti-ATF3, mouse anti-cyclin E (1:1000, Santacruz biotech), rabbit anti-cyclin D1, anti-cyclin A, (1:1000, Thermo Scientific), anti-HSPA2 (1:1000, ProteinTech), anti-phospho-p38 MAPK (Thr180/Tyr182), or anti-phospho ERK (Ser21/9) antibodies (1:1000, Cell Signaling Technology). SuperSignal West Femto Maximum Sensitivity Chemiluminescence Substrate (Pierce) was used for detection, and the blots were normalized to endogenous p38 and ERK-44/42 MAPKs, β-actin, and GAPDH (1:1000, Cell Signaling Technology).

Immunolocalization

Spermatocytes were serum starved for 24 h on a 4-chambered slide (Nalge Nunc) and treated with 0.1% DMSO or CSC (100 μg/ml) for 2 h. Following incubation, the cells were fixed in 4% paraformaldehyde for 5 min, blocked in 2% BSA and 10% normal serum, incubated overnight with rabbit anti-NRF2, anti-ATF3, and mouse anti-E2F4 antibodies (1:50) (Santacruz biotech), washed with PBS, incubated with Alexa Fluor 488-conjugated goat anti-rabbit or Alexa Fluor 546-conjugated anti-mouse (1:500; Life Technologies) secondary antibody for 1 h, and counterstained with TO-PRO-3 iodide (1:500, Life Technologies) for 5 min. Fluorescence was observed by confocal microscopy (Nikon Eclipse E800). Negative control without primary antibody was used to confirm the specificity of staining. Signal intensity was measured by using Image J 1.45s.

Image analysis

Image J software 1.45s (NIH) was used for image analysis, which was performed as previously described (Esakky et al., 2012). A minimum of 50 replicate fields were analyzed for each biological specimen.

Statistical analyses

Data from three independent experiments each assayed in duplicates or triplicates are represented as mean ± SEM. The qRT-PCR data were analyzed by using either two-tailed unpaired *t*-tests or one-way ANOVA (nonparametric) followed by Tukey's multiple comparison test with 95% confidence intervals. Prism 5.0d (GraphPad) was used, and $P < 0.05$ was considered statistically significant.

Acknowledgements

The authors gratefully thank Dr Deborah Frank (Washington University School of Medicine) for her suggestions and scientific writing expertise. We thank the Alvin J. Siteman Cancer Center at Washington University School of Medicine and Barnes-Jewish Hospital in St. Louis, MO, USA, for the use of the Siteman Flow Cytometry Core, which provided cell-sorting services. The Siteman Cancer Center is supported in part by an NCI Cancer Center Support Grant.

Funding

This material is based upon work supported by the Department of Veterans Affairs, Veterans Health Administration, Biomedical Laboratory Research and Development Award # I01BX007080.

Conflict of interest: none declared.

References

Abdelrahim, M., Smith, R., III, and Safe, S. (2003). Aryl hydrocarbon receptor gene silencing with small inhibitory RNA differentially modulates Ah-responsiveness in MCF-7 and HepG2 cancer cells. Mol. Pharmacol. *63*, 1373–1381.

Aitken, R.J., and Baker, M.A. (2004). Oxidative stress and male reproductive biology. Reprod. Fertil. Dev. *16*, 581–588.

Barnes-Ellerbe, S., Knudsen, K.E., and Puga, A. (2004). 2,3,7,8-Tetrachlorodibenzo-p-dioxin blocks androgen-dependent cell proliferation of LNCaP cells through modulation of pRB phosphorylation. Mol. Pharmacol. *66*, 502–511.

Bustin, S.A., Benes, V., Garson, J.A., et al. (2009). The MIQE guidelines—minimum information for publication of quantitative real-time PCR experiments. Clin. Chem. *55*, 611–622.

Chen, Z.H., Kim, H.P., Sciurba, F.C., et al. (2008). Egr-1 regulates autophagy in cigarette smoke-induced chronic obstructive pulmonary disease. PLoS One *3*, e3316.

Davis, R.J. (2000). Signal transduction by the JNK group of MAP kinases. Cell *103*, 239–252.

Deschênes, C., Alvarez, L., Lizotte, M.E., et al. (2004). The nucleocytoplasmic shuttling of E2F4 is involved in the regulation of human intestinal epithelial cell proliferation and differentiation. J. Cell. Physiol. *199*, 262–273.

Dudley, D.T., Pang, L., Decker, S.J., et al. (1995). A synthetic inhibitor of the mitogen activated protein kinase cascade. Proc. Natl Acad. Sci. USA *92*, 7686–7689.

Elizondo, G., Fernandez-Salguero, P., Sheikh, M.S., et al. (2000). Altered cell cycle control at the G(2)/M phases in aryl hydrocarbon receptor-null embryo fibroblast. Mol. Pharmacol. *57*, 1056–1063.

Esakky, P., Hansen, D.A., Drury, A.M., et al. (2012). Cigarette smoke condensate induces aryl hydrocarbon receptor-dependent changes in gene expression in spermatocytes. Reprod. Toxicol. *34*, 665–676.

Esakky, P., Hansen, D.A., Drury, A.M., et al. (2013). Molecular analysis of cell type-specific gene expression profile during mouse spermatogenesis by laser microdissection and qRT-PCR. Reprod. Sci. *3*, 238–252.

Esakky, P., Hansen, D.A., Drury, A.M., et al. (2014). Modulation of cell cycle progression in the spermatocyte cell line [GC-2spd(ts) Cell-Line] by cigarette smoke condensate (CSC) via arylhydrocarbon receptor-nuclear factor erythroid 2-related factor 2 (Ahr-Nrf2) pathway. Biol. Reprod. *90*, 1–12.

Fields, W.R., Leonard, R.M., Odom, P.S., et al. (2005). Gene expression in normal human bronchial epithelial (NHBE) cells following in vitro exposure to cigarette smoke condensate. Toxicol. Sci. *86*, 84–91.

Garneau, H., Paquin, M.C., Carrier, J.C., et al. (2009). E2F4 expression is required for cell cycle progression of normal intestinal crypt cells and colorectal cancer cells. J. Cell. Physiol. *221*, 350–358.

Ge, N.L., and Elferink, C.J. (1998). A direct interaction between the aryl hydrocarbon receptor and retinoblastoma protein. Linking dioxin signaling to the cell cycle. J. Biol. Chem. *28*, 22708–22713.

Georgellis, A., Montelius, J., and Rydström, J. (1987). Evidence for a free-radical-dependent metabolism of 7,12-dimethylbenz[a]anthracene in rat testis. Toxicol. Appl. Pharmacol. *87*, 141–154.

Gierthy, J.F., and Crane, D. (1984). Reversible inhibition of in vitro epithelial cell proliferation by 2,3,7,8-tetrachlorodibenzo-p-dioxin. Toxicol. Appl. Pharmacol. *15*, 91–98.

Gratzner, H.G. (1982). Monoclonal antibody to 5-bromo- and 5-iododeoxyuridine: a new reagent for detection of DNA replication. Science *218*, 474–475.

Hai, T., Wolfgang, C.D., Marsee, A.K., et al. (1999). ATF3 and stress responses. Gene Exp. *7*, 321–335.

Henklová, P., Vrzal, R., Ulrichová, J., et al. (2008). Role of mitogen-activated protein kinases in aryl hydrocarbon receptor signaling. Chem. Biol. Interact. *172*, 93–104.

Hoffman, E.C., Reyes, H., Chu, F.F., et al. (1991). Cloning of a factor required for activity of the Ah (dioxin) receptor. Science *252*, 954–958.

Janz, M., Hummel, M., Truss, M., et al. (2006). Classical Hodgkin lymphoma is characterized by high constitutive expression of activating transcription factor 3 (ATF3), which promotes viability of Hodgkin/Reed-Sternberg cells. Blood *107*, 2536–2539.

Jeong, G.S., Lee, D.S., Li, B., et al. (2010). Protective effect of sauchinone by upregulating heme oxygenase-1 via the p38 MAPK and Nrf2/ARE pathways in HepG2 cells. Planta Med. *76*, 41–47.

Jin, M.H., Hong, C.H., Lee, H.Y., et al. (2008). Enhanced TGF-β1 is involved in 2,3,7,8-tetrachlorodibenzo-p-dioxin (TCDD) induced oxidative stress in C57BL/6 mouse testis. Toxicol. Lett. *178*, 202–209.

Kim, S.H., Henry, E.C., Kim, D.K., et al. (2006). Novel compound 2-methyl-2H-pyrazole-3-carboxylic acid (2-methyl-4-o-tolylazo-phenyl)-amide (CH-223191) prevents 2,3,7,8-TCDD-induced toxicity by antagonizing the aryl hydrocarbon receptor. Mol. Pharmacol. *69*, 1871–1878.

Kim, K., Jeong, J., Surh, Y., et al. (2010). Expression of stress-response ATF3 is mediated by Nrf2 in astrocytes. Nucleic Acids Res. *38*, 48–59.

Korashy, H.M., Anwar-Mohamed, A., Soshilov, A.A., et al. (2011). The p38 MAPK inhibitor SB203580 induces cytochrome P450 1A1 gene expression in murine and human hepatoma cell lines through ligand-dependent Aryl hydrocarbon receptor activation. Chem. Res. Toxicol. *24*, 1540–1548.

Krutzik, P.O., Clutter, M.R., and Nolan, G.P. (2005). Coordinate analysis of murine immune cell surface markers and intracellular phosphoproteins by flow cytometry. J. Immunol. *175*, 2357–2365.

Kumar, M.B., Tarpey, R.W., and Perdew, G.H. (1999). Differential recruitment of coactivator RIP140 by Ah and estrogen receptors. Absence of a role for LXXLL motifs. J. Biol. Chem. *274*, 22155–22164.

Lindeman, G.J., Gaubatz, S., Livingston, D.M., et al. (1997). The subcellular localization of E2F-4 is cell-cycle dependent. Proc. Natl Acad. Sci. USA *94*, 5095–5100.

Livak, K.J., and Schmittgen, T.D. (2001). Analysis of relative gene expression data using real time quantitative PCR and the $2^{-\Delta\Delta CT}$ method. Methods *25*, 402–408.

Lu, D., Wolfgang, C.D., and Hai, T. (2006). Activating transcription factor 3, a stress-inducible gene, suppresses Ras-stimulated tumorigenesis. J. Biol. Chem. *281*, 10473–10481.

Lu, D., Chen, J., and Ha, T. (2007). The regulation of ATF3 gene expression by mitogen-activated protein kinases. Biochem. J. *401*, 559–567.

Ma, Q., and Whitlock, J.P., Jr. (1996). The aromatic hydrocarbon receptor modulates the Hepa 1c1c7 cell cycle and differentiated state independently of dioxin. Mol. Cell. Biol. *16*, 2144–2150.

Massague, J., Seoane, J., and Wotton, D. (2005). Smad transcription factors. Genes Dev. *19*, 2783–2810.

Nagaraj, N.S., Beckersa, S., Mensaha, J.K., et al. (2006). Cigarette smoke condensate induces cytochromes P450 and aldo-keto reductases in oral cancer cells. Toxicol. Lett. *165*, 182–194.

Patel, R.D., Kim, D.J., Peters, J.M., et al. (2006). The aryl hydrocarbon receptor directly regulates expression of the potent mitogen epiregulin. Toxicol. Sci. *89*, 75–82.

Pollenz, R.Z., and Buggy, Z. (2006). Ligand-dependent and -independent degradation of the human arylhydrocarbon receptor (hAHR) in cell culture models. Chem. Biol. Interact. *164*, 49–59.

Puga, A., Barnes, S.J., Dalton, T.P., et al. (2000). Aromatic hydrocarbon receptor interaction with the retinoblastoma protein potentiates repression of E2F-dependent transcription and cell cycle arrest. J. Biol. Chem. *275*, 2943–2950.

Ramlau-Hansen, C.H., Thulstrup, A.M., Aggerholm, A.S., et al. (2007). Is smoking a risk factor for decreased semen quality? A cross-sectional analysis. Hum. Reprod. *22*, 188–196.

Reddy, N.M., Kleeberger, S.R., and Bream, J.H. (2008). Genetic disruption of the Nrf2 compromises cell-cycle progression by impairing GSH-induced redox signaling. Oncogene *27*, 5821–5832.

Ren, B., Cam, H., Takahashi, Y., et al. (2002). E2F integrates cell cycle progression with DNA repair, replication, and G2/M checkpoints. Genes Dev. *16*, 245–256.

Rutault, K., Hazzalin, C.A., and Mahadevan, L.C. (2001). Combinations of ERK and p38 MAPK inhibitors ablate tumor necrosis factor-α (TNF-α) mRNA induction. Evidence for selective destabilization of TNF-α transcripts. J. Biol. Chem. *276*, 6666–6674.

Salic, A., and Mitchison, T.J. (2008). A chemical method for fast and sensitive detection of DNA synthesis in vivo. Proc. Natl Acad. Sci. USA *105*, 2415–2420.

Smith, C.J., and Hansch, C. (2000). The relative toxicity of compounds in mainstream cigarette smoke condensate. Food Chem. Toxicol. *38*, 637–646.

Smith, C.J., Perfetti, T.A., Garg, R., et al. (2003). IARC carcinogens reported in cigarette mainstream smoke and their calculated log P values. Food Chem. Toxicol. *41*, 807–817.

Tan, Z., Chang, X., Puga, A., et al. (2002). Activation of mitogen-activated protein kinases (MAPKs) by aromatic hydrocarbons: role in the regulation

of aryl hydrocarbon receptor (AHR) function. Biochem. Pharmacol. *64*, 771–780.

Venugopal, R., and Jaiswal, A.K. (1996). Nrf1 and Nrf2 positively and c-Fos and Fra1 negatively regulate the human antioxidant response element-mediated expression of NAD(P)H:quinone oxidoreductase1 gene. Proc. Natl Acad. Sci. USA *93*, 14960–14965.

Weiss, C., Kolluri, S.K., Kiefer, F., et al. (1996). Complementation of Ah receptor deficiency in hepatoma cells: negative feedback regulation and cell cycle control by the Ah receptor. Exp. Cell Res. *226*, 154–163.

Weiss, C., Faust, D., Durk, H., et al. (2005). TCDD induces c-jun expression via a novel Ah (dioxin) receptor-mediated p38-MAPK-dependent pathway. Oncogene *24*, 4975–4983.

Wolkowicz, M.J., Coonrod, S.A., Reddi, P.P., et al. (1996). Refinement of the differentiated phenotype of the spermatogenic cell line GC-2spd(ts). Biol. Reprod. *55*, 923–932.

Zordoky, B.N., and El-Kadi, A.O. (2009). Role of NF-kappaB in the regulation of cytochrome p450 enzymes. Curr. Drug Metab. *10*, 164–178.